

Revisiting Gauge-Independent Kinetic Energy Densities in Meta-GGAs and Local Hybrid Calculations of Magnetizabilities

Caspar J. Schattenberg,[†] Artur Wodyński,[†] Hugo Åström,[‡] Dage Sundholm,[‡]
Martin Kaupp,^{*,†} and Susi Lehtola^{*,‡,¶}

[†]*Technische Universität Berlin, Institut für Chemie, Theoretische Chemie/Quantenchemie, Sekr. C7, Straße des 17. Juni 135, D-10623, Berlin, Germany*

[‡]*University of Helsinki, Department of Chemistry, Faculty of Science, P.O. Box 55 (A.I. Virtanens plats 1), FI-00014 University of Helsinki, Finland*

[¶]*Molecular Sciences Software Institute, Blacksburg, Virginia 24061, United States*

E-mail: martin.kaupp@tu-berlin.de; susi.lehtola@alumni.helsinki.fi

Abstract

In a recent study [J. Chem. Theory Comput. 2021, 17, 1457–1468], some of us examined the accuracy of magnetizabilities calculated with density functionals representing the local density approximation (LDA), generalized gradient approximation (GGA), meta-GGA (mGGA) as well as global hybrid (GH) and range-separated (RS) hybrid functionals by assessment against accurate reference values obtained with coupled-cluster theory with singles, doubles and perturbative triples [CCSD(T)]. Our study was later extended to local-hybrid (LH) functionals by Holzer et al. [J. Chem. Theory Comput. 2021, 17, 2928–2947]; in this work, we examine a larger selection of LH functionals, also including range-separated LH (RSLH) functionals and strong-correlation LH (scLH) functionals. Holzer et al also studied the importance of the physically correct handling of the magnetic gauge dependence of the kinetic energy density (τ) in mGGA calculations by comparing the Maximoff–Scuseria formulation of τ used in our aforementioned study to the more physical current-density extension derived by Dobson. In this work, we also revisit this comparison with a larger selection of mGGA

functionals. We find that the newly tested LH, RSLH and scLH functionals outperform all the functionals considered in the previous studies. The various LH functionals afford the seven lowest mean absolute errors, while also showing remarkably small standard deviations and mean errors. Most strikingly, the best two functionals are scLHs that also perform remarkably well in cases with significant multiconfigurational character such as the ozone molecule, which is traditionally excluded from the statistical error evaluation due to its large errors with common density functionals.

1 Introduction

Molecular magnetic properties such as nuclear magnetic resonance (NMR) shielding constants, NMR spin-spin coupling constants, and magnetizabilities are useful probes of molecular and electronic structure, and they can be studied to pinpoint the location of atoms in a molecule, for instance. However, interpreting the measured spectra often requires computational modeling. Quantum chemical modeling of magnetic properties is often pursued using Kohn–Sham (KS) density functional theory^{1,2} (DFT).^{3–10} However, the accuracy of DFT for some of these

properties has not been thoroughly established in the literature. Some of us recently employed the benchmark set of ref. 7 to assess the accuracy of density functionals^{11,12} with an emphasis on newer functionals from rungs 2–4 of the usual Jacob’s ladder hierarchy;¹³ this benchmark set consists of magnetizabilities for 28 small main-group molecules computed with coupled-cluster theory with singles, doubles and perturbative triples [CCSD(T)], which is a highly accurate wave function theory (WFT).

It was found in ref. 11 that the BHandHLYP¹⁴ global hybrid (GH) functional and some range-separated hybrid (RSH) functionals provided the closest agreement with the CCSD(T) reference data, with the smallest mean absolute deviations (MADs) being slightly above $3 \times 10^{-30} \text{ J/T}^2$, while Hartree–Fock gave $7.22 \times 10^{-30} \text{ J/T}^2$ and was ranked 29th best out of 52 methods evaluated.^{11,12} Some functionals, in particular of the highly parameterized Minnesota functionals, were found to reach MADs with large errors above $10 \times 10^{-30} \text{ J/T}^2$.

Our study in refs. 11 and 12 employed TURBOMOLE,^{15,16} which until recently relied on the Maximoff–Scuseria (MS) approach¹⁷ to turn the kinetic energy density τ used in meta-generalized gradient approximation (mGGA) functionals into a gauge-independent quantity in the presence of a magnetic field. However, recent work by some of us has shown that the MS approach that is also used in the GAUSSIAN¹⁸ program may lead to artefacts for nuclear magnetic shielding constants, such as artificial paramagnetic contributions to the shielding constant of spherical atoms, which can be avoided by employing Dobson’s current-density extension of τ ,¹⁹ instead;^{20–23} this approach is nowadays available in TURBOMOLE for time-dependent density functional theory (TDDFT) calculations^{24–26} and other properties.^{27,28} The approach is also used in other packages as well for TDDFT and NMR calculations.^{29,30} We also note that Dobson’s current-density extension for τ has been found to be important in the context of calculations in explicit magnetic fields.^{31–35}

Holzer et al.²⁷ recently employed the method-

ology of refs. 11 and 12 to compare the effect of the MS and Dobson formulations of τ on the magnetizabilities of two test sets: the aforementioned theory-based test set of ref. 7, and a test set based on experimental data. Their results appeared at first sight somewhat inconclusive, as the two test sets resulted in different rankings of various functionals.

Several local hybrid (LH) functionals that employ a position-dependent exact-exchange (EXX) admixture^{36,37} and that have been shown to exhibit promising accuracy for nuclear magnetic shielding constants^{20–23} performed excellently for the theory-based test set, with relative mean absolute deviations in magnetizabilities below 1 %. However, Holzer et al.²⁷ put more emphasis on the comparison to experimental data, in which deviations for most functionals including LH functionals were generally above 5 % and were less systematic than in the theory-based benchmark.

We argue that the comparison to these experimental data does not afford a reliable assessment of the accuracy of density functionals, as many of these data exhibit large error bars. As LH functionals are of interest for many kinds of properties, we revisit their performance for magnetizabilities in this work, based on the theoretical dataset of Lutnæs et al.⁷ which was also used in previous studies.^{11,12,27} Although the limitations of this kind of static DFT benchmarks need to be recognized,³⁸ such studies often give helpful guidance in terms of the suitable physical contents of density functional approximations.

Going beyond the LH functionals studied in ref. 27, we also include the first modern range-separated local hybrid (RSLH) ω LH22t³⁹ in our assessment, as it has been shown to provide remarkable accuracy for quasiparticle energies of a wide variety of organic chromophores of interest in molecular electronics and organic photovoltaics,⁴⁰ while also performing well for many other ground- and excited-state properties.³⁹ We also investigate the performance of recent strong-correlation-corrected LH functionals (scLH) such as scLH22t and scLH22ta,⁴¹ as well as the most recent models with simplified constructions of the sc-correction terms.⁴²

We will show that these functionals can more reliably reproduce magnetizabilities of systems with large static correlation effects such as O_3 , whose magnetizabilities predicted by regular LH functionals significantly deviate from the CCSD(T) reference value.²⁷

In addition, we will also study the Dobson formulation for τ on a wider set of τ -dependent functionals than those studied in ref. 27, including various older and newer mGGA functionals and mGGA-based global and range-separated hybrid functionals.

The layout of this work is as follows. Next, in section 2, we will discuss the employed methodology for computing the magnetizability (section 2.1), gauge origin problems (section 2.2), and LH functionals (section 2.3), and then the employed computational methodology in section 3. We present the results of this study in section 4, and conclude in section 5. Atomic units are used throughout, unless specified otherwise.

2 Theory

2.1 Methods for Calculating Magnetizabilities

Magnetizabilities are commonly calculated as the second derivative of the electronic energy with respect to the external magnetic field^{9,43–46}

$$\xi_{\alpha\beta} = - \left. \frac{\partial^2 E}{\partial B_\alpha \partial B_\beta} \right|_{\mathbf{B}=\mathbf{0}}. \quad (1)$$

The magnetic interaction can also be expressed as an integral over the magnetic interaction energy density $\rho^{\mathbf{B}}(\mathbf{r})$, which is the scalar product of the magnetically induced current density $\mathbf{J}^{\mathbf{B}}(\mathbf{r})$ with the vector potential $\mathbf{A}^{\mathbf{B}}(\mathbf{r})$ of the external magnetic field \mathbf{B} ^{11,12,47–53}

$$E = \int \rho^{\mathbf{B}}(\mathbf{r}) \, d^3r = -\frac{1}{2} \int \mathbf{A}^{\mathbf{B}}(\mathbf{r}) \cdot \mathbf{J}^{\mathbf{B}}(\mathbf{r}) \, d^3r. \quad (2)$$

The second derivatives of the magnetic interaction energy with respect to the components of the external magnetic field, together forming the elements of the magnetizability tensor $\boldsymbol{\xi}$,

can be obtained from eq. (2) as an integral over the scalar product of the first derivatives of the vector potential of the external magnetic field with the magnetically induced current-density susceptibility (CDT), $\partial J_\gamma^{\mathbf{B}}(\mathbf{r})/\partial B_\beta|_{\mathbf{B}=\mathbf{0}}$, in the limit of a vanishing magnetic field^{52–54}

$$\xi_{\alpha\beta} = \frac{1}{2} \int \left. \frac{\partial \mathbf{A}^{\mathbf{B}}(\mathbf{r})}{\partial B_\alpha} \cdot \frac{\partial \mathbf{J}^{\mathbf{B}}(\mathbf{r})}{\partial B_\beta} \, d^3r \right|_{\mathbf{B}=\mathbf{0}}, \quad (3)$$

where the vector potential $\mathbf{A}^{\mathbf{B}}(\mathbf{r})$ of a homogeneous external magnetic field is

$$\mathbf{A}^{\mathbf{B}}(\mathbf{r}) = \frac{1}{2} \mathbf{B} \times (\mathbf{r} - \mathbf{R}_O) \quad (4)$$

and \mathbf{R}_O is an arbitrary gauge origin. The CDT can be calculated in a given atomic-orbital (AO) basis set from the unperturbed and the magnetically perturbed AO density matrices, which can be obtained at any level of theory from nuclear magnetic shielding calculations, for example.^{55–58}

The isotropic magnetizability ($\bar{\xi}$) is obtained as one third of the trace of the magnetizability tensor

$$\bar{\xi} = \frac{1}{3} \text{Tr} \boldsymbol{\xi} = \int \bar{\rho}^\xi(\mathbf{r}) \, d^3r, \quad (5)$$

where the magnetizability density tensor is defined in terms of the CDT as

$$\rho_{\alpha\beta}^\xi(\mathbf{r}) = \frac{1}{2} \sum_{\delta\gamma} \epsilon_{\alpha\delta\gamma} r_\delta \left. \frac{\partial J_\gamma^{\mathbf{B}}(\mathbf{r})}{\partial B_\beta} \right|_{\mathbf{B}=\mathbf{0}}, \quad (6)$$

where $\epsilon_{\alpha\delta\gamma}$ is the Levi–Civita symbol, and $\alpha, \beta, \gamma, \delta$ and $r_\delta \in \{x, y, z\}$ are Cartesian directions. The $\xi_{\alpha\alpha}, \alpha \in \{x, y, z\}$ elements of the magnetizability tensor can be obtained by quadrature as

$$\xi_{\alpha\alpha} = \sum_{i=1}^n w_i \rho_{i;\alpha\alpha}^\xi \quad (7)$$

where $\rho_{i;\alpha\alpha}^\xi$ is a diagonal element of the magnetizability density tensor at quadrature point i and w_i is the corresponding quadrature weight.

The use of the above quadrature scheme allows magnetizabilities to be computed even when the analytical second derivatives required to evaluate eq. (1) are not available.¹¹ In addition to providing a complementary approach

to computing magnetizabilities, the numerical integration approach also affords information about spatial contributions to the magnetizability; ^{11,12} similar approaches have previously also been used to study spatial contributions to nuclear magnetic shielding constants. ^{59–68}

2.2 Gauge-Origin Problems

The use of a finite one-particle basis set introduces issues with gauge dependence into quantum chemical calculations of magnetic properties. The CDT can be made gauge-origin independent ^{55,57,58,69} by using gauge-including atomic orbitals (GIAOs), ^{4,70–73} also known as London atomic orbitals (LAOs), ^{43,46,74}

$$\chi_\mu(\mathbf{r}) = e^{-i(\mathbf{B} \times [\mathbf{R}_\mu - \mathbf{R}_O] \cdot \mathbf{r}) / (2c)} \chi_\mu^{(0)}(\mathbf{r}), \quad (8)$$

where i is the imaginary unit, $\chi_\mu^{(0)}(\mathbf{r})$ is a basis function centered at \mathbf{R}_μ , and c is the speed of light which has the value $c = \alpha^{-1} \approx 137.036$ in atomic units, where α is the fine-structure constant.

The mGGA approximation for the exchange-correlation energy density contains a dependence on the kinetic energy density τ , which reads in the field-free case as

$$\tau(\mathbf{r}) = \frac{1}{2} \sum_{\mu\nu} D_{\mu\nu} \nabla \chi_\mu^*(\mathbf{r}) \cdot \nabla \chi_\nu(\mathbf{r}), \quad (9)$$

where $D_{\mu\nu}$ is the AO density matrix. However, this dependence requires additional care, as the (uncorrected) $\tau(\mathbf{r})$ of eq. (9) is clearly not *a priori* gauge invariant even when using GIAOs.

A widely used model to render $\tau(\mathbf{r})$ gauge-invariant was introduced by Maximoff and Scuseria ¹⁷ (MS) as

$$\tau_{\text{MS}}(\mathbf{r}) = \tau(\mathbf{r}) + \frac{1}{c} (\mathbf{A}^{\mathbf{B}}) \cdot \mathbf{j}_p(\mathbf{r}) + \frac{|\mathbf{A}^{\mathbf{B}}|^2}{c^2} \rho(\mathbf{r}), \quad (10)$$

where $\mathbf{j}_p(\mathbf{r})$ is the paramagnetic current density defined as

$$\mathbf{j}_p(\mathbf{r}) = \frac{i}{2} \sum_{\mu\nu} D_{\mu\nu} (\chi_\nu \nabla \chi_\mu^* - \chi_\mu^* \nabla \chi_\nu). \quad (11)$$

Advantages for coupled-perturbed KS

(CPKS) calculations with mGGAs arise from the diagonality of the Hessian for $\tau_{\text{MS}}(\mathbf{r})$, which allows solving the CPKS equations in a single step. However, the semi-local exchange-correlation (XC) contribution does not produce a linear response, even though a genuine current-density functional is expected to provide such a response. ^{75,76} $\tau_{\text{MS}}(\mathbf{r})$ also does not constitute a proper iso-orbital indicator, ⁷⁷ is non-universal, ^{24,33,78} and introduces paramagnetic artefacts in shielding calculations. ²⁰

A formulation that avoids the disadvantages of the MS model was proposed by Dobson ^{19,79}

$$\tau_{\text{D}}(\mathbf{r}) = \tau(\mathbf{r}) - \frac{|\mathbf{j}_p(\mathbf{r})|^2}{2\rho(\mathbf{r})}. \quad (12)$$

$\tau_{\text{D}}(\mathbf{r})$ in eq. (12) leads to gauge independence, while also introducing a current-response of the semi-local XC contribution and thereby a correct physical behavior for τ -dependent density functionals. As the electronic Hessian corresponding to eq. (12) is non-diagonal, an iterative solution to the CPKS equations is now necessary, rendering the calculations slightly more expensive than when the physically incorrect eq. (10) is used.

2.3 Local Hybrid Functionals

In addition to studying the importance of the Dobson formulation (eq. (12)) of the kinetic-energy density in reproducing accurate magnetizabilities, we will also evaluate the accuracy of LH functionals. A form for an LH functional that emphasizes the inclusion of nonlocal correlation terms (often considered to cover nondynamical correlation, NDC) together with full exact exchange and a (semi-local) dynamical correlation (DC) functional is ^{13,37}

$$\begin{aligned} E_{\text{XC}}^{\text{LH}} &= E_{\text{X}}^{\text{ex}} + \int (1 - g(\mathbf{r})) \times \\ &\quad (e_{\text{X}}^{\text{sl}}(\mathbf{r}) + G(\mathbf{r}) - e_{\text{X}}^{\text{ex}}(\mathbf{r})) \, \text{d}\mathbf{r} + E_{\text{C}} \\ &= E_{\text{X}}^{\text{ex}} + E_{\text{NDC}} + E_{\text{DC}}, \end{aligned} \quad (13)$$

where $g(\mathbf{r})$ is the local mixing function (LMF) controlling the fraction of exact exchange included at \mathbf{r} . In most of the LH functionals con-

sidered here we use a so-called t-LMF defined as the scaled ratio between the von Weizsäcker⁸⁰ and KS kinetic energy densities

$$g(\mathbf{r}) = a \cdot \frac{\tau_W(\mathbf{r})}{\tau(\mathbf{r})}, \quad \tau_W(\mathbf{r}) = \frac{|\nabla\rho(\mathbf{r})|^2}{8\rho(\mathbf{r})}. \quad (14)$$

The calibration function (CF) $G(\mathbf{r})$ is used in eq. (13) to correct for the ambiguity of the semi-local and exact exchange-energy densities.^{37,81–84} In the LH functionals with a CF from the Berlin group,^{39,41,85} the semi-local CFs are currently derived within the partial integration gauge (pig) approach.⁸³

We also evaluate two recent extensions of LH functionals: the so-called strong-correlation-corrected LH functionals (scLH)^{41,42,86} and a range-separated local hybrid (RSLH) functional (ω LH22t).³⁹ In the scLH functionals, a strong-correlation factor $q_{AC}(\mathbf{r})$ is introduced into the LMF of the LH:

$$E_{XC}^{scLH} = E_X^{ex} + 2 \int q_{AC}(\mathbf{r}) \cdot \left[(1 - g(\mathbf{r})) \times (e_X^{sl}(\mathbf{r}) + G(\mathbf{r}) - e_X^{ex}(\mathbf{r})) + e_C(\mathbf{r}) \right] d\mathbf{r}. \quad (15)$$

This approach is based on the local adiabatic connection approach, and is adapted from the KP16/B13⁸⁷ and B13⁸⁸ sc-models. The most recent models employ simplified real-space measures to detect strong correlations, as well as modified damping functions to avoid double-counting of NDC contributions in more weakly correlated situations.⁴²

In the absence of strong correlations, $q_{AC} \rightarrow 0.5$ as a lower bound, and the underlying LH functional is restored. Whenever the quantities underlying q_{AC} detect locally the presence of strong correlations, q_{AC} is increased, maximally up to 1.0. In the exchange picture, this means that the EXX admixture is locally diminished; in some cases it may even become negative.^{41,42} This enhances the simulation of nonlocal correlation contributions and is crucial for reducing fractional spin errors and for improving spin-restricted bond dissociation curves.^{41,42}

RSLH functionals like ω LH22t³⁹ may be writ-

ten as

$$E_{XC}^{LH} = E_X^{ex} + \int (1 - g(\mathbf{r})) \times (e_{X,SR}^{sl}(\mathbf{r}) + G(\mathbf{r}) - e_{X,SR}^{ex}(\mathbf{r})) d\mathbf{r} + E_C, \quad (16)$$

where $e_{X,SR}^{sl}$ and $e_{X,SR}^{ex}$ are short-range exchange-energy densities, controlled by the range-separation parameter ω . In consequence, the ω LH22t functional has full long-range EXX admixture,³⁹ like the RSH functionals evaluated here as well, while the short-range EXX admixture is determined by the LMF.

3 Computational Methods

As in refs. 11 and 12, the unperturbed and magnetically perturbed density matrices are generated with the nuclear magnetic shielding module of the TURBOMOLE program (`mpshift`).¹⁶ A locally modified version of TURBOMOLE 7.6 has been used for the present calculations. TURBOMOLE employs LIBXC⁸⁹ to evaluate many of the presently considered density functionals. A detailed description of the implementations of the LH functionals,²⁰ the Dobson model,²³ and higher derivatives of the density used in the pig2 CF²¹ can be found in the respective publications. The necessary equations for the magnetic-field derivatives of scLHs and RSLHs are outlined in Section S1 of the Supporting Information.

The calculations were carried out with the aug-cc-pCVQZ basis set^{90–95} (with aug-cc-pVQZ on hydrogen atoms) employing GIAOs^{71,72,74,96} a.k.a. LAOs.^{43,46} The self-consistent field convergence criteria were set as 10^{-9} for the energy and 10^{-7} for the density. Large numerical integration grids per the approach of Becke⁹⁷ were used with the TURBOMOLE^{15,16} setting `gridsize` 7, following the original work of Treutler and Ahlrichs⁹⁸ with later extensions documented in the TURBOMOLE manual.⁹⁹ The non-standard exact-exchange integrals occurring in LH, scLH and RSLH functionals are calculated by efficient semi-numerical integration techniques,^{100–103}

using standard DFT grids.

The resolution-of-the-identity (RI) approximation was used to evaluate the Coulomb contribution (J), using Turbomole’s “universal” auxiliary basis set by Weigend.¹⁰⁴ Although one needs to be careful about mixing auxiliary basis sets for different families, we tested the accuracy of this RI-J approximation with a few of the functionals considered in this work, and the resulting magnetizabilities with the RI-J approximation coincided with values obtained without it to the reported number of digits, which is consistent with results recently computed for NMR shieldings.^{105,106} We note that accurate auxiliary basis sets with controllable accuracy for RI calculations can nowadays be easily generated automatically,^{107,108} and recommend such autogenerated auxiliary basis sets to be used when tailored basis sets are not available. We refer the reader to ref. 109 for a recent review of further automatical auxiliary basis generation techniques.

The magnetizabilities are computed from the density matrices produced by TURBOMOLE with the GIMIC program.^{55–58} The integral in eq. (6) is calculated in GIMIC using Becke’s⁹⁷ multicenter quadrature scheme,^{11,12} employing the NUMGRID library¹¹⁰ to generate the atomic quadrature grids with a hardness parameter of 3 for the atomic weight partitioning, radial grids from Lindh et al.¹¹¹ and Lebedev’s angular grids.¹¹² Both GIMIC and NUMGRID are free and open-source software.^{113,114}

In this work, we study the accuracy of magnetizabilities reproduced by the 31 functionals listed in table 1 for a dataset of 28 molecules: AlF, C₂H₄, C₃H₄, CH₂O, CH₃F, CH₄, CO, FCCH, FCN, H₂C₂O, H₂O, H₂S, H₄C₂O, HCN, HCP, HF, HFCO, HOF, LiF, LiH, N₂, N₂O, NH₃, O₃, OCS, OF₂, PN, and SO₂, which have also been used as benchmark molecules in other studies.^{7,11,12} The obtained DFT magnetizabilities are compared to the CCSD(T) reference values of ref. 7. Since the magnetizability for O₃ introduces significant uncertainties due to large static correlation effects, it was omitted from the statistical analysis, as was also done in refs. 11 and 12.

4 Results

We will begin the discussion of the results in section 4.1 by examining the accuracy of all the considered functionals with the Dobson and MS models for τ in the subset of data without O₃, which exhibits strong correlation effects. We then discuss the accuracy of the various functionals O₃ in section 4.2. The magnetizabilities for all studied molecules and functionals with the MS and Dobson formulations of τ can be found in the Supporting Information (SI), accompanied with violin plots of the corresponding error distributions.

4.1 Accuracy of Density Functionals with Various Models for τ

Table 2 summarizes the overall statistical evaluations and the ranking of the various functionals within the Dobson and the MS models for τ . We begin by noting that our results agree with those of Holzer et al.²⁷ for the subset of functionals also studied in ref. 27.

In the mean absolute error (MAE) analysis, the largest effects of using τ_D instead of τ_{MS} are obtained for some Minnesota functionals, *e.g.*, -5.47×10^{-30} J/T² for MN15, -2.38×10^{-30} J/T² for M06-2X, and $+1.69 \times 10^{-30}$ J/T² for M06. Other functionals that exhibit large (more than 0.5×10^{-30} J/T²) effects on the MAEs include PW6B95 (-0.72×10^{-30} J/T²) and MN15-L ($+0.52 \times 10^{-30}$ J/T²). We note here that many Minnesota functionals, including M06 and M06-2X, have been recently found to be numerically ill-behaved, while MN15 and MN15-L appear to behave better.^{137,138}

The MAE values suggest that ensuring proper gauge invariance may either improve or worsen the agreement with the CCSD(T) reference data. Some of us have found a similar behavior for NMR chemical shifts,^{22,23} and attributed it to massive error compensation in some of the cases.

However, in most cases the differences between the MS and Dobson formulations are small, and the rankings of the best-performing functionals are not affected very much by

Table 1: The employed local-hybrid functionals (LH), range-separated LH functionals (RSLH), strong correlation LH functionals (scLH), functionals at the meta-generalized gradient approximation (mGGA), global hybrid (GH) functionals as well as range-separated (RS) GGA and mGGA functionals, and one GGA functional

Functional	Type	Notes	References
scLH23t-mBR ^a	scLH	ct-LMF ($a \approx 0.715$), damped q_{AC-erf} , pig2-CF, $X_{0.22S+0.78PBE+C_{modB95}}$	42
scLH23t-mBR-P ^a	scLH	ct-LMF ($a \approx 0.715$), damped $q_{AC-Pad\acute{e}}$, pig2-CF, $X_{0.22S+0.78PBE+C_{modB95}}$	42
scLH22t	scLH	ct-LMF ($a = 0.715$), damped q_{AC} , pig2-CF, $X_{0.22S+0.78PBE+C_{modB95}}$	41
scLH22ta	scLH	ct-LMF ($a = 0.766$), q_{AC} , pig2-CF, $X_{0.04S+0.96PBE+C_{modB95}}$	41
scLH21ct-SVWN-m	scLH	ct-LMF ($a = 0.628$), q_{AC} , X_S+C_{VWN}	86
ω LH22t	RSLH	ct-LMF ($a = 0.587$), $\omega = 0.233$, pig2-CF, $X_{PBE+C_{modB95}}$	39
LH20t	LH	ct-LMF ($a = 0.715$), pig2-CF, $X_{0.22S+0.78PBE+C_{modB95}}$	85
LH20t nonCal	LH	ct-LMF ($a = 0.715$), $X_{0.22S+0.78PBE+C_{modB95}}$	85
LH14t-calPBE	LH	t-LMF ($a = 0.5$), pig1-CF, $X_{0.49S+0.51PBE+C_{0.55PW92+0.45PBE}}$	115
LH12ct-SsirPW92	LH	ct-LMF ($a = 0.646$), $X_S+C_{sicPW92}$	116
LH12ct-SsifPW92	LH	ct-LMF ($a = 0.709$), $X_S+C_{sicPW92}$	116
LH07t-SVWN	LH	t-LMF ($a = 0.48$), X_S+C_{VWN}	117,118
LH07s-SVWN	LH	s-LMF ($b = 0.277$), X_S+C_{VWN}	119
mPSTS-a1 ^b	LH	modified PSTS functional	27,120
mPSTS-noa2 ^b	LH	modified PSTS functional	27,120
LHJ14	LH	z-LMF ($c = 0.096$), $X_{B88}+C_{B88}$	121
B97M-V	mGGA		122
VSXC	mGGA		123
MN15-L	mGGA		124
TPSS	mGGA		125,126
M06-L	mGGA		127
τ -HCTH	mGGA		128
PW6B95	GH, mGGA		129
TPSSh	GH, mGGA		125,126
M06-2X	GH, mGGA		130
M06	GH, mGGA		130
MN15	GH, mGGA		131
B3LYP5 ^c	GH, GGA		132,133
BHandHLYP	GH, GGA		134
ω B97M-V	RSH, mGGA		135
ω B97X-V	RSH, GGA		136

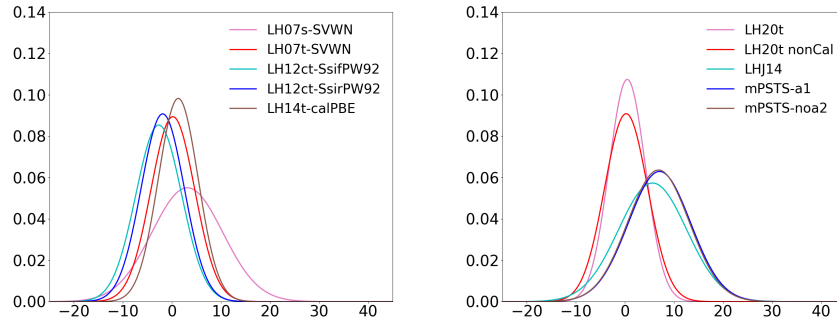
^a Use of simplified q_{AC} based on error function (scLH23t-mBR) or Padé functions (scLH23t-mBR-P); simplified construction of underlying function to identify regions of strong-correlation; see ref. 42 for details

^b See ref. 27 for further details of the a1 and noa2 models

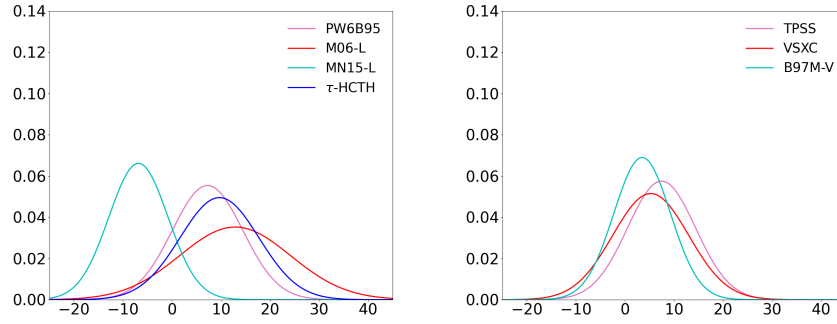
^c This functional is called B3LYP in TURBOMOLE, and as discussed by Hertwig and Koch,¹³³ it is slightly different from the B3LYP functional used in ref. 11.

Table 2: Mean absolute errors (MAEs), mean errors (MEs), and standard deviations (STDs) of the errors in the magnetizabilities of the 27 studied molecules in units of 10^{-30} J/T² from the CCSD(T) reference values with the studied functionals

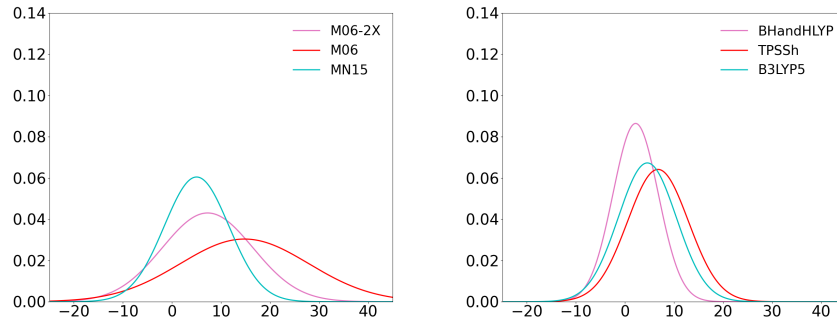
Rank	Functional	MAE	ME	STD	Rank	MAE	ME	STD
			τ_D				τ_{MS}	
1	scLH23t-mBR	2.25	-0.31	3.40	1	2.39	0.36	3.78
2	scLH22t	2.35	-0.29	3.27	2	2.47	0.47	3.62
3	LH20t	2.48	0.46	3.71	4	2.71	1.15	4.09
4	scLH23t-mBR-P	2.52	-0.41	3.81	3	2.69	0.27	4.20
5	scLH22ta	2.67	0.24	3.64	5	2.83	0.66	3.78
6	LH14t-calPBE	3.02	1.28	4.06	8	3.21	2.06	4.21
7	ω LH22t	3.09	0.12	4.06	10	3.49	1.16	4.73
8	BHandHLYP	3.13	2.17	4.61	7	3.13	2.17	4.61
9	ω B97X-V	3.23	2.53	4.31	9	3.23	2.53	4.31
10	LH20t nonCal	3.31	0.23	4.39	14	3.68	1.74	4.97
11	LH07t-SVWN	3.55	0.18	4.46	13	3.68	2.01	4.72
12	scLH21ct-SVWN-m	3.61	-2.73	3.46	6	3.07	-0.15	3.99
13	LH12ct-SsirPW92	3.74	-1.89	4.39	11	3.59	0.14	4.63
14	ω B97M-V	3.87	1.40	5.03	12	3.62	0.43	4.70
15	LH12ct-SsifPW92	4.25	-2.70	4.67	15	3.93	-0.67	4.94
16	B97M-V	4.78	3.50	5.79	16	5.19	4.13	5.48
17	B3LYP5	5.44	4.55	5.93	17	5.44	4.55	5.93
18	LH07s-SVWN	5.84	3.12	7.24	18	5.84	3.12	7.24
19	MN15	6.00	5.02	6.60	29	11.47	10.46	12.63
20	TPSSh	6.82	6.73	6.22	23	7.22	7.09	5.97
21	mPSTS-noa2	6.85	6.83	6.27	22	7.15	7.13	5.99
22	VSXC	6.96	5.24	7.75	20	7.07	5.50	7.52
23	LHJ14	6.98	5.62	6.96	21	7.13	5.56	7.55
24	MN15-L	7.07	-6.84	6.04	19	6.55	-5.25	6.81
25	mPSTS-a1	7.10	7.04	6.34	24	7.42	7.37	6.07
26	PW6B95	7.60	7.26	7.20	26	8.32	8.00	8.10
27	M06-2X	7.80	7.26	9.27	28	10.18	9.03	12.93
28	TPSS	7.83	7.46	6.94	25	8.24	7.88	6.77
29	τ -HCTH	10.20	9.68	8.06	27	9.74	9.22	7.83
30	M06-L	12.93	12.86	11.32	30	12.53	12.49	9.30
31	M06	15.06	14.78	13.12	31	13.37	13.14	12.98



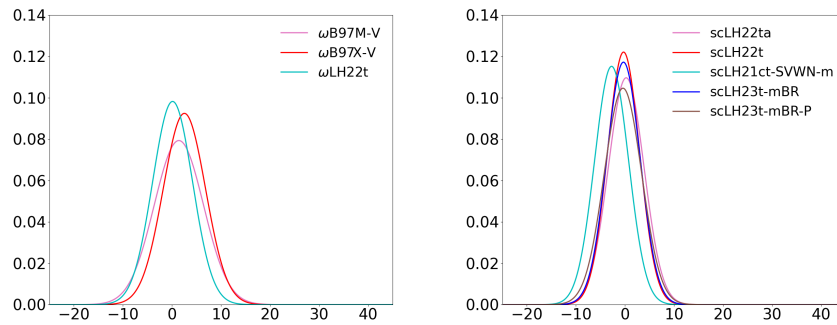
(a) LH functionals



(b) mGGA functionals



(c) GH functionals



(d) RSH and scLH functionals

Figure 1: Normal distributions of the magnetizability data calculated with the Dobson formulation of τ .

switching from using the MS expression to the Dobson expression. Some exceptions do occur; for instance the change of $-0.40 \times 10^{-30} \text{ J/T}^2$ going from τ_{MS} to τ_{D} leads to an improved ranking by three positions for ωLH22t .

Interesting differences can be seen between the behavior of some first-generation LH functionals based on LSDA exchange-energy densities (*e.g.*, LH12ct-SsirPW92, LH12ct-SsifPW92, and the related scLH21ct-SVWN-m) and that of the more advanced functionals (LH, scLH, and the ωLH22t RSLH functional). The accuracy of functionals of the former type deteriorates somewhat after switching from the computationally convenient τ_{MS} to the physically more correct τ_{D} , while the accuracy of the latter type of functionals improves when τ_{D} is used.

A closer analysis of the origin of the differences between the MS and Dobson formulations of τ is beyond the scope of this work. However, a recent study of the Dobson-based gauge-invariance contributions to TDDFT excitation energies has been able to link the magnitude and even the sign of the effect to the way in which τ enters the enhancement factor of the mGGA functionals and other τ -dependent functionals.²⁶

LH20t and its sc-corrected extensions scLH22t and scLH23t-mBR occupy ranks 3, 2 and 1, respectively, with the scLHs improving slightly over their parent LH functional. The reduced MAE of scLH23t-mBR and scLH22t as compared to LH20t arises from some of the molecules that are expected to exhibit larger static correlation effects, as evidenced by larger deviations between CCSD(T) and CCSD results in Ref. 7. Apart from the true static correlation case O_3 (see below), scLH22t gives notable improvements of more than $2 \times 10^{-30} \text{ J/T}^2$ for PN and SO_2 . scLH23t-mBR gives large improvements for PN and HCP. The performance of both functionals would be even more impressive if not for the somewhat larger deviations of $-6.4 \times 10^{-30} \text{ J/T}^2$ (scLH22t) and $-5.3 \times 10^{-30} \text{ J/T}^2$ for the LiH molecule as compared to the LH20t value of $+3.2 \times 10^{-30} \text{ J/T}^2$. scLH23t-mBR-P, with its Padé-based q_{AC} also improves particularly on PN and HCP but

deteriorates on LiH ($-10.6 \times 10^{-30} \text{ J/T}^2$), hampering the functionals’s overall statistical performance compared to the other two scLHs and leaves it slightly behind LH20t in the overall ranking. Effects of the sc-corrections are much smaller for the other molecules, which is consistent with an efficient damping of the sc-factor for weakly correlated systems. It is presently unclear why the effects of the sc-corrections are below $1 \times 10^{-30} \text{ J/T}^2$ for several other systems with larger differences between CCSD and CCSD(T) (H_2CO , OF_2 , HOF).

The two best-performing functionals in refs. 11 and 12 (BHandHLYP and $\omega\text{B97X-V}$) are ranked 8th and 9th when considering the Dobson formulation of τ . Strikingly, several LH and scLH functionals, as well as the ωLH22t RSLH functional occupy the seven top positions in the ranking, and several further LH functionals follow in the top 15 of the ranking (table 2). A similar trend was observed earlier when considering a smaller selection of LH functionals.²⁷ However, somewhat different conclusions were then reached because the experimental data used as reference values in that work exhibit very large error bars and are therefore ill-suited for benchmarking purposes.

Individual changes from LH20t to scLH22ta which lacks the damping factor are overall somewhat more pronounced and lead to a slightly larger MAE for the scLH functionals, indicating some deterioration of the accuracy of the magnetizability for more weakly correlated systems, which places scLH22ta behind LH20t, but scLH22ta is still ranked 5th best.

Further top-performing functionals include LH14t-calPBE (rank 6) and the ωLH22t RSLH (rank 7), but their MAE in the $3.0\text{-}3.3 \times 10^{-30} \text{ J/T}^2$ range is already comparable to those of the best-performing functionals from refs. 11 and 12 (BHandHLYP, $\omega\text{B97X-V}$, and CAM-QTP functionals). In agreement with refs. 11 and 12, B97M-V remains the highest-ranked non-hybrid functional in the evaluations, its MAE is reduced from $5.19 \times 10^{-30} \text{ J/T}^2$ to $4.78 \times 10^{-30} \text{ J/T}^2$ by using the Dobson formulation of τ . The normal distributions of the magnetizabilities of the studied functionals with the Dobson formula for τ are shown in

fig. 1; analogous plots for the MS formula for τ are given in the SI, along with violin plots of the errors for both descriptions, both with and without the inclusion of O_3 in the data set.

4.2 Accuracy on O_3

As was already discussed above, due to its large static correlation effects, O_3 has been excluded from statistical evaluations in previous density functional assessments.^{7,11,12} Its large deviations would otherwise dominate the statistics and it is unclear whether the CCSD(T) reference value is sufficiently accurate for this molecule, given that the inclusion of the perturbational triples (T) contributions reduces the magnetizability by more than $45 \times 10^{-30} \text{ J/T}^2$ as compared to the CCSD value.⁷ In the absence of experimental data, we may estimate a reasonable range of values by also considering earlier complete active space self-consistent field (CASSCF) GIAO ($97.8 \times 10^{-30} \text{ J/T}^2$)¹³⁹ and multiconfigurational (MC) individual gauge for localized orbitals (IGLO) ($89.7 \times 10^{-30} \text{ J/T}^2$)¹⁴⁰ results. These values are somewhat smaller than the CCSD(T) reference value of $121.5 \times 10^{-30} \text{ J/T}^2$ and suggest that magnetizabilities around $100 \times 10^{-30} \text{ J/T}^2$ with an error margin of about $\pm 20 \times 10^{-30} \text{ J/T}^2$ seem to define the most likely range. We review the various DFT results in light of this range in table 3.

Most functionals overestimate the magnetizability of O_3 dramatically. Among the standard functionals studied here and in refs. 11 and 12, the specialized GGA functionals like KT1, KT2, and KT3 get closest to the reference value, with KT1 providing the smallest value of $131.9 \times 10^{-30} \text{ J/T}^2$. These DFAs are not good performers in general according to the previous magnetizability benchmark,^{11,12} and would enter at ranks 19, 21, and 31 with MAE of $5.87 \times 10^{-30} \text{ J/T}^2$, $6.42 \times 10^{-30} \text{ J/T}^2$ and $9.19 \times 10^{-30} \text{ J/T}^2$, respectively, in the statistical evaluation of table 2. Other standard GGA functionals like BLYP or BP86 give magnetizabilities of O_3 around $180 \times 10^{-30} \text{ J/T}^2$.¹¹ Similar results for simple GGA functionals were also obtained in the original evaluation of Lutnæs et al.⁷ However, these functionals perform

poorly for the entire test set, which is why we will not discuss them further here. Some mGGA functionals like M06-L and B97M-V also attain closer agreement when the τ_{MS} prescription is used, but using the more appropriate τ_{D} results in larger magnetizability and leads to a poorer agreement. When the Dobson formulation is used, most mGGA functionals perform comparably to the simpler GGA functionals, with TPSS and τ -HCTH giving the lowest values of $173.5 \times 10^{-30} \text{ J/T}^2$ and $178.5 \times 10^{-30} \text{ J/T}^2$, respectively.

Table 3: Calculated isotropic magnetizabilities [10^{-30} J/T^2] for ozone with various methods.

Functional	Type	$\xi[O_3]$	
		τ_{D}	τ_{MS}
B3LYP	GH, GGA	238.5	
BHandHLYP	GH, GGA	336.6	
B97M-V	mGGA	189.8	99.3
M06-L	mGGA	244.2	156.2
MN15-L	mGGA	193.7	63.6
PW6B95	mGGA	261.4	288.3
τ -HCTH	mGGA	178.3	177.0
TPSS	mGGA	173.5	151.1
VSXC	mGGA	193.9	155.3
M06	GH, mGGA	417.8	413.4
MN15	GH, mGGA	259.5	570.8
M06-2X	GH, mGGA	328.1	492.9
TPSSh	GH, mGGA	200.1	176.9
ω B97X-V	RSH, GGA	251.2	
ω B97M-V	RSH, mGGA	239.8	225.3
LH07s-SVWN	LH	256.0	
LH07t-SVWN	LH	211.2	207.3
LH12ct-SsifPW92	LH	221.6	227.4
LH12ct-SsirPW92	LH	218.2	220.2
LH14t-calPBE	LH	207.5	207.2
LH20t	LH	211.4	223.1
LH20t nonCal	LH	217.3	229.9
LHJ14	LH	213.6	244.3
mPSTS-a1	LH	198.9	175.5
mPSTS-noa2	LH	207.5	183.8
scLH22ct-SVWN-m	scLH	112.9	90.8
scLH22ta	scLH	101.0	90.8
scLH22t	scLH	112.2	109.5
scLH23t-mBR	scLH	120.4	121.4
scLH23t-mBR-P	scLH	134.4	136.5
ω LH22t	RSLH	224.9	240.9
CCSD(T)-GIAO ^a	WFT	121.5	
CASSCF-GIAO ^b	WFT	97.8	
MC-IGLO ^c	WFT	89.7	

^a ref. 11; ^b ref. 139; ^c ref. 140

Including exact exchange in GH and RSH functionals significantly increases the calcu-

lated magnetizability of ozone, and thereby deteriorates the agreement with the reference value, in some cases they are more than $300 \times 10^{-30} \text{ J/T}^2$ (BHandHLYP, M06, M06-2X). We find a similar trend for all LH functionals without sc-corrections as well as for the ω LH22t RSLH functional that yield values larger than $200 \times 10^{-30} \text{ J/T}^2$. The strikingly good performance of various scLH functionals is thus particularly notable: scLH22ta without damping factor in the sc-corrections gives the lowest value, results for the other sc-functionals are in the range of $112 - 135 \times 10^{-30} \text{ J/T}^2$.

Given that four of the five scLHs are also among the five best-performing functionals for the entire test set, these results are significant in suggesting that the scLH functionals to some extent indeed escape the usual zero-sum game between delocalization errors and strong-correlation errors, where larger EXX admixtures improve on the former but deteriorate the latter.¹⁴¹ Such an “escape” has been found recently for fractional spin errors and the related spin-restricted dissociation curves of diatomics.^{41,42} It is gratifying to see this here for a very different property.

5 Conclusions

This work extends in two directions previous studies of DFT functionals for the computation of molecular magnetizabilities. We considered using a gauge-independent local kinetic energy τ ingredient in a wide variety of mGGA functionals within Dobson’s current-DFT formalism (τ_D), which had not been considered in as much detail so far. We examined the effects of the Dobson formalism by comparing the obtained magnetizabilities to values calculated with the Maximoff–Scuseria (MS) formulation (τ_{MS}) used in previous works. We also extended the assessment to local hybrid functionals *i.e.*, with position-dependent exact-exchange admixtures, in particular to their recent strong-correlation corrected and range-separated variants.

Regarding gauge invariant formulations of τ , we find that going from the previously used,

computationally convenient τ_{MS} to the more physically correct τ_D leads in some cases to dramatic changes in the magnetizability, while in other cases the differences between τ_D and τ_{MS} are small. The largest effects are seen for some of the highly parameterized mGGA and mGGA hybrid functionals from the Minnesota group, whose numerical behavior has also been recently investigated and found wanting for many functionals.^{137,138}

While τ_D leads to improved agreement with the CCSD(T) reference data for some functionals, it also deteriorates the agreement for other functionals. Notably, the effects of making τ gauge-invariant by the Dobson procedure tend to be smaller for the overall better-performing functionals, which include many local and range-separated hybrid functionals.

The overall statistical evaluation of a wide variety of different functionals provided evidence that local hybrid functionals can yield particularly accurate magnetizabilities. Indeed, the seven best-performing functionals in the present evaluation are newer local hybrid functionals, their strong-correlation corrected variants, and the recently reported range-separated local hybrid functional ω LH22t. The overall statistical improvement compared to the so far best-performing functionals is moderate but notable, *e.g.*, MAEs of $2.25 \times 10^{-30} \text{ J/T}^2$, $2.35 \times 10^{-30} \text{ J/T}^2$ and $2.48 \times 10^{-30} \text{ J/T}^2$ for scLH23t-mBR, scLH22t and LH20t, respectively, compared to $3.11 \times 10^{-30} \text{ J/T}^2$ for BHandHLYP and $3.23 \times 10^{-30} \text{ J/T}^2$ for ω B97X-V.

The most striking result is the dramatic improvement obtained with several of the strong-correlation corrected local hybrid functionals for the static-correlation case O_3 . Importantly, this improvement is achieved while retaining the overall highest accuracy for the weakly correlated systems relevant for the statistical evaluations. This observation for a totally different property than evaluated so far for such functionals is a further indication that strong-correlation corrected local hybrid functionals offer an escape from the usual zero-sum game between achieving low fractional charge errors and low fractional spin errors.

Acknowledgement This work has been supported by the Academy of Finland through project numbers 340583, 350282, and 353749, by Magnus Ehrnrooth Foundation, the Finnish Society of Sciences and Letters and by the Swedish Cultural Foundation in Finland. We acknowledge computational resources from CSC—IT Center for Science, Finland. Work in Berlin has been supported by DFG project KA1187/15-1.

Supporting Information Available

Magnetizabilities, normal distributions and violin plots of the error distributions of the magnetizabilities calculated with the Maximoff–Scuseria and Dobson expressions of τ . Equations necessary to implement the magnetic field derivatives for sLHs and RSLHs.

References

- (1) Hohenberg, P.; Kohn, W. Inhomogeneous Electron Gas. *Phys. Rev.* **1964**, *136*, B864–B871.
- (2) Kohn, W.; Sham, L. J. Self-Consistent Equations Including Exchange and Correlation Effects. *Phys. Rev.* **1965**, *140*, A1133–A1138.
- (3) Helgaker, T.; Jaszuński, M.; Ruud, K. Ab Initio Methods for the Calculation of NMR Shielding and Indirect Spin–Spin Coupling Constants. *Chem. Rev.* **1999**, *99*, 293–352.
- (4) Gauss, J.; Stanton, J. F. Electron-Correlated Approaches for the Calculation of NMR Chemical Shifts. *Adv. Chem. Phys.* **2002**, *123*, 355–422.
- (5) Keal, T. W.; Tozer, D. J.; Helgaker, T. GIAO shielding constants and indirect spin–spin coupling constants: performance of density functional methods. *Chem. Phys. Lett.* **2004**, *391*, 374–379.
- (6) Gauss, J.; Ruud, K.; Kállay, M. Gauge-origin independent calculation of magnetizabilities and rotational g tensors at the coupled-cluster level. *J. Chem. Phys.* **2007**, *127*, 074101.
- (7) Lutnæs, O. B.; Teale, A. M.; Helgaker, T.; Tozer, D. J.; Ruud, K.; Gauss, J. Benchmarking density-functional-theory calculations of rotational g tensors and magnetizabilities using accurate coupled-cluster calculations. *J. Chem. Phys.* **2009**, *131*, 144104.
- (8) Teale, A. M.; Lutnæs, O. B.; Helgaker, T.; Tozer, D. J.; Gauss, J. Benchmarking density-functional theory calculations of NMR shielding constants and spin-rotation constants using accurate coupled-cluster calculations. *J. Chem. Phys.* **2013**, *138*, 024111.
- (9) Loibl, S.; Schütz, M. Magnetizability and rotational g tensors for density fitted local second-order Møller–Plesset perturbation theory using gauge-including atomic orbitals. *J. Chem. Phys.* **2014**, *141*, 024108.
- (10) Reimann, S.; Borgoo, A.; Tellgren, E. I.; Teale, A. M.; Helgaker, T. Magnetic-Field Density-Functional Theory (BDFT): Lessons from the Adiabatic Connection. *J. Chem. Theory Comput.* **2017**, *13*, 4089–4100.
- (11) Lehtola, S.; Dimitrova, M.; Fliegl, H.; Sundholm, D. Benchmarking Magnetizabilities with Recent Density Functionals. *J. Chem. Theory Comput.* **2021**, *17*, 1457–1468.
- (12) Lehtola, S.; Dimitrova, M.; Fliegl, H.; Sundholm, D. Correction to "Benchmarking Magnetizabilities with Recent Density Functionals". *J. Chem. Theory Comput.* **2021**, *17*, 4629–4631.
- (13) Perdew, J. P.; Schmidt, K. Jacob’s ladder of density functional approximations for the exchange-correlation energy. *AIP Conf. Proc.* **2001**, *577*, 1–20.
- (14) Becke, A. D. A new mixing of Hartree–Fock and local density-functional theories. *J. Chem. Phys.* **1993**, *98*, 1372–1377.
- (15) Balasubramani, S. G.; Chen, G. P.; Coriani, S.; Diedenhofen, M.; Frank, M. S.; Franzke, Y. J.; Furche, F.; Grotjahn, R.; Harding, M. E.; Hättig, C. et al. TURBOMOLE: Modular program suite for ab initio quantum-chemical and condensed-matter simulations. *J. Chem. Phys.* **2020**, *152*, 184107.
- (16) TURBOMOLE V7.6 2021, a development of University of Karlsruhe and Forschungszentrum Karlsruhe GmbH, 1989-2007, TURBOMOLE GmbH, since 2007; available from <https://www.turbomole.org>.

- (17) Maximoff, S. N.; Scuseria, G. E. Nuclear magnetic resonance shielding tensors calculated with kinetic energy density-dependent exchange-correlation functionals. *Chem. Phys. Lett.* **2004**, *390*, 408–412.
- (18) Frisch, M. J.; Trucks, G. W.; Schlegel, H. B.; Scuseria, G. E.; Robb, M. A.; Cheeseman, J. R.; Scalmani, G.; Barone, V.; Petersson, G. A.; Nakatsuji, H. et al. Gaussian 16 Revision C.01. 2016; Gaussian Inc. Wallingford CT.
- (19) Dobson, J. F. Alternative expressions for the Fermi hole curvature. *J. Chem. Phys.* **1993**, *98*, 8870–8872.
- (20) Schattenberg, C. J.; Kaupp, M. Effect of the Current Dependence of Tau-Dependent Exchange-Correlation Functionals on Nuclear Shielding Calculations. *J. Chem. Theory Comput.* **2021**, *17*, 1469–1479.
- (21) Schattenberg, C. J.; Kaupp, M. Implementation and Validation of Local Hybrid Functionals with Calibrated Exchange-Energy Densities for Nuclear Shielding Constants. *J. Phys. Chem. A* **2021**, *125*, 2697–2707.
- (22) Schattenberg, C. J.; Kaupp, M. Extended Benchmark Set of Main-Group Nuclear Shielding Constants and NMR Chemical Shifts and Its Use to Evaluate Modern DFT Methods. *J. Chem. Theory Comput.* **2021**, *17*, 7602–7621.
- (23) Schattenberg, C. J.; Lehmann, M.; Bühl, M.; Kaupp, M. Systematic Evaluation of Modern Density Functional Methods for the Computation of NMR Shifts of 3d Transition-Metal Nuclei. *J. Chem. Theory Comput.* **2021**, *18*, 273–292.
- (24) Bates, J. E.; Furche, F. Harnessing the meta-generalized gradient approximation for time-dependent density functional theory. *J. Chem. Phys.* **2012**, *137*, 164105.
- (25) Bates, J. E.; Heiche, M. C.; Liang, J.; Furche, F. Erratum: "Harnessing the meta-generalized gradient approximation for time-dependent density functional theory" [J. Chem. Phys. 137, 164105 (2012)]. *J. Chem. Phys.* **2022**, *156*, 159902.
- (26) Grotjahn, R.; Furche, F.; Kaupp, M. Importance of imposing gauge invariance in time-dependent density functional theory calculations with meta-generalized gradient approximations. *J. Chem. Phys.* **2022**, *157*, 111102.
- (27) Holzer, C.; Franzke, Y. J.; Kehry, M. Assessing the Accuracy of Local Hybrid Density Functional Approximations for Molecular Response Properties. *J. Chem. Theory Comput.* **2021**, *17*, 2928–2947.
- (28) Franzke, Y. J.; Holzer, C. Impact of the current density on paramagnetic NMR properties. *J. Chem. Phys.* **2022**, *157*, 031102.
- (29) Liang, J.; Feng, X.; Hait, D.; Head-Gordon, M. Revisiting the Performance of Time-Dependent Density Functional Theory for Electronic Excitations: Assessment of 43 Popular and Recently Developed Functionals from Rungs One to Four. *J. Chem. Theory Comput.* **2022**, *18*, 3460–3473.
- (30) Neese, F. Software update: The ORCA program system—Version 5.0. *WIREs Comput. Mol. Sci.* **2022**, *12*, e1606.
- (31) Tellgren, E. I.; Teale, A. M.; Furness, J. W.; Lange, K. K.; Ekström, U.; Helgaker, T. Non-perturbative calculation of molecular magnetic properties within current-density functional theory. *J. Chem. Phys.* **2014**, *140*, 034101.
- (32) Furness, J. W.; Verbeke, J.; Tellgren, E. I.; Stopkowicz, S.; Ekström, U.; Helgaker, T.; Teale, A. M. Current Density Functional Theory Using

- Meta-Generalized Gradient Exchange-Correlation Functionals. *J. Chem. Theory Comput.* **2015**, *11*, 4169–4181.
- (33) Reimann, S.; Ekström, U.; Stopkowitz, S.; Teale, A. M.; Borgoo, A.; Helgaker, T. The importance of current contributions to shielding constants in density-functional theory. *Phys. Chem. Chem. Phys.* **2015**, *17*, 18834–18842.
- (34) Irons, T. J. P.; Spence, L.; David, G.; Speake, B. T.; Helgaker, T.; Teale, A. M. Analyzing Magnetically Induced Currents in Molecular Systems Using Current-Density-Functional Theory. *J. Phys. Chem. A* **2020**, *124*, 1321–1333.
- (35) Irons, T. J. P.; David, G.; Teale, A. M. Optimizing Molecular Geometries in Strong Magnetic Fields. *J. Chem. Theory Comput.* **2021**, *17*, 2166–2185.
- (36) Jaramillo, J.; Scuseria, G. E.; Ernzerhof, M. Local hybrid functionals. *J. Chem. Phys.* **2003**, *118*, 1068–1073.
- (37) Maier, T. M.; Arbuznikov, A. V.; Kaupp, M. Local hybrid functionals: Theory, implementation, and performance of an emerging new tool in quantum chemistry and beyond. *Wiley Interdiscip. Rev. Comput. Mol. Sci.* **2019**, *9*, e1378.
- (38) Weymuth, T.; Reiher, M. The transferability limits of static benchmarks. *Phys. Chem. Chem. Phys.* **2022**, *24*, 14692–14698.
- (39) Fürst, S.; Haasler, M.; Grotjahn, R.; Kaupp, M. Full Implementation, Optimization, and Evaluation of a Range-Separated Local Hybrid Functional with Wide Accuracy for Ground and Excited States. *J. Chem. Theory Comput.* **2023**, *19*, 488–502.
- (40) Fürst, S.; Kaupp, M. Accurate ionization potentials, electron affinities and band gaps from the ω LH22t range-separated local hybrid functional: no tuning required. *J. Chem. Theory Comput.* **2023**,
- (41) Wodyński, A.; Kaupp, M. Local Hybrid Functional Applicable to Weakly and Strongly Correlated Systems. *J. Chem. Theory Comput.* **2022**, *18*, 6111–6123.
- (42) Wodyński, A.; Arbuznikov, A. V.; Kaupp, M. Strong-correlation density functionals made simple. *J. Chem. Phys.* **2023**, *158*, 244117.
- (43) Ruud, K.; Helgaker, T.; Bak, K. L.; Jørgensen, P.; Jensen, H. J. A. Hartree–Fock limit magnetizabilities from London orbitals. *J. Chem. Phys.* **1993**, *99*, 3847.
- (44) Ruud, K.; Skaane, H.; Helgaker, T.; Bak, K. L.; Jørgensen, P. Magnetizability of Hydrocarbons. *J. Am. Chem. Soc.* **1994**, *116*, 10135–10140.
- (45) Ruud, K.; Helgaker, T.; Bak, K. L.; Jørgensen, P.; Olsen, J. Accurate magnetizabilities of the isoelectronic series BeH^- , BH , and CH^+ . The MCSCF-GIAO approach. *Chem. Phys.* **1995**, *195*, 157–169.
- (46) Helgaker, T.; Coriani, S.; Jørgensen, P.; Kristensen, K.; Olsen, J.; Ruud, K. Recent advances in wave function-based methods of molecular-property calculations. *Chem. Rev.* **2012**, *112*, 543–631.
- (47) Stevens, R. M.; Pitzer, R. M.; Lipscomb, W. N. Perturbed Hartree–Fock Calculations. I. Magnetic Susceptibility and Shielding in the LiH Molecule. *J. Chem. Phys.* **1963**, *38*, 550–560.
- (48) Jameson, C. J.; Buckingham, A. D. Nuclear magnetic shielding density. *J. Phys. Chem.* **1979**, *83*, 3366–3371.
- (49) Jameson, C. J.; Buckingham, A. D. Molecular electronic property density functions: The nuclear magnetic shielding density. *J. Chem. Phys.* **1980**, *73*, 5684–5692.

- (50) Fowler, P. W.; Steiner, E.; Cadioli, B.; Zanasi, R. Distributed-gauge calculations of current density maps, magnetizabilities, and shieldings for a series of neutral and dianionic fused tetracycles: pyracylene ($C_{14}H_8$), acepleiadylene ($C_{16}H_{10}$), and dipleiadiene ($C_{18}H_{12}$). *J. Phys. Chem. A* **1998**, *102*, 7297–7302.
- (51) Iliáš, M.; Jensen, H. J. A.; Bast, R.; Saue, T. Gauge origin independent calculations of molecular magnetisabilities in relativistic four-component theory. *Mol. Phys.* **2013**, *111*, 1373–1381.
- (52) Lazzeretti, P. Ring currents. *Prog. Nucl. Magn. Reson. Spectrosc.* **2000**, *36*, 1–88.
- (53) Lazzeretti, P. Current density tensors. *J. Chem. Phys.* **2018**, *148*, 134109.
- (54) Sambe, H. Properties of induced electron current density of a molecule under a static uniform magnetic field. *J. Chem. Phys.* **1973**, *59*, 555–555.
- (55) Jusélius, J.; Sundholm, D.; Gauss, J. Calculation of current densities using gauge-including atomic orbitals. *J. Chem. Phys.* **2004**, *121*, 3952–3963.
- (56) Taubert, S.; Sundholm, D.; Jusélius, J. Calculation of spin-current densities using gauge-including atomic orbitals. *J. Chem. Phys.* **2011**, *134*, 054123.
- (57) Fliegl, H.; Taubert, S.; Lehtonen, O.; Sundholm, D. The gauge including magnetically induced current method. *Phys. Chem. Chem. Phys.* **2011**, *13*, 20500.
- (58) Sundholm, D.; Fliegl, H.; Berger, R. J. Calculations of magnetically induced current densities: theory and applications. *Wiley Interdiscip. Rev.: Comput. Mol. Sci.* **2016**, *6*, 639–678.
- (59) Steiner, E.; Fowler, P. W. On the orbital analysis of magnetic properties. *Phys. Chem. Chem. Phys.* **2004**, *6*, 261–272.
- (60) Pelloni, S.; Ligabue, A.; Lazzeretti, P. Ring-current models from the differential Biot–Savart law. *Org. Lett.* **2004**, *6*, 4451–4454.
- (61) Ferraro, M. B.; Lazzeretti, P.; Viglione, R. G.; Zanasi, R. Understanding proton magnetic shielding in the benzene molecule. *Chem. Phys. Lett.* **2004**, *390*, 268–271.
- (62) Soncini, A.; Fowler, P.; Lazzeretti, P.; Zanasi, R. Ring-current signatures in shielding-density maps. *Chem. Phys. Lett.* **2005**, *401*, 164–169.
- (63) Ferraro, M. B.; Faglioni, F.; Ligabue, A.; Pelloni, S.; Lazzeretti, P. Ring current effects on nuclear magnetic shielding of carbon in the benzene molecule. *Magn. Reson. Chem.* **2005**, *43*, 316–320.
- (64) Acke, G.; Van Damme, S.; Havenith, R. W. A.; Bultinck, P. Interpreting the behavior of the NICS_{zz} by resolving in orbitals, sign, and positions. *J. Comput. Chem.* **2018**, *39*, 511–519.
- (65) Acke, G.; Van Damme, S.; Havenith, R. W. A.; Bultinck, P. Quantifying the conceptual problems associated with the isotropic NICS through analyses of its underlying density. *Phys. Chem. Chem. Phys.* **2019**, *21*, 3145–3153.
- (66) Jinger, R. K.; Fliegl, H.; Bast, R.; Dimitrova, M.; Lehtola, S.; Sundholm, D. Spatial Contributions to Nuclear Magnetic Shieldings. *J. Phys. Chem. A* **2021**, *125*, 1778–1786.
- (67) Fliegl, H.; Dimitrova, M.; Berger, R. J. F.; Sundholm, D. Spatial Contributions to 1H NMR Chemical Shifts of Free-Base Porphyrinoids. *Chemistry* **2021**, *3*, 1005–1021.
- (68) Summa, F. F.; Monaco, G.; Zanasi, R. Decomposition of Molecular Integrals into Atomic Contributions via Becke Partitioning Scheme: a Caveat. *Croat. Chem. Acta* **2021**, *94*, 43–46.

- (69) Sundholm, D.; Dimitrova, M.; Berger, R. J. F. Current density and molecular magnetic properties. *Chem. Commun.* **2021**, *57*, 12362–12378.
- (70) Hamerka, H. F. Theory of Magnetic Properties of Molecules with Particular Emphasis on the Hydrogen Molecule. *Rev. Mod. Phys.* **1962**, *34*, 87–101.
- (71) Ditchfield, R. Self-consistent perturbation theory of diamagnetism. I. A gauge-invariant LCAO method for N.M.R. chemical shifts. *Mol. Phys.* **1974**, *27*, 789–807.
- (72) Wolinski, K.; Hinton, J. F.; Pulay, P. Efficient implementation of the gauge-independent atomic orbital method for NMR chemical shift calculations. *J. Am. Chem. Soc.* **1990**, *112*, 8251–8260.
- (73) Gauss, J. Calculation of NMR chemical shifts at second-order many-body perturbation theory using gauge-including atomic orbitals. *Chem. Phys. Lett.* **1992**, *191*, 614–620.
- (74) London, F. Théorie quantique des courants interatomiques dans les combinaisons aromatiques. *J. Phys. le Radium* **1937**, *8*, 397–409.
- (75) Vignale, G.; Rasolt, M. Density-functional theory in strong magnetic fields. *Phys. Rev. Lett.* **1987**, *59*, 2360–2363.
- (76) Vignale, G.; Rasolt, M. Current- and spin-density-functional theory for inhomogeneous electronic systems in strong magnetic fields. *Phys. Rev. B* **1988**, *37*, 10685–10696.
- (77) Sagvolden, E.; Ekstrm, U.; Tellgren, E. I. Isoorbital indicators for current density functional theory. *Mol. Phys.* **2013**, *111*, 1295–1302.
- (78) Tao, J. Explicit inclusion of paramagnetic current density in the exchange-correlation functionals of current-density functional theory. *Phys. Rev. B* **2005**, *71*, 205107.
- (79) Dobson, J. F. Spin-density functionals for the electron correlation energy with automatic freedom from orbital self-interaction. *J. Phys.: Condens. Matter* **1992**, *4*, 7877–7890.
- (80) von Weizsäcker, C. F. Zur Theorie der Kernmassen. *Z. Phys.* **1935**, *96*, 431.
- (81) Burke, K.; Cruz, F. G.; Lam, K.-C. Unambiguous exchange-correlation energy density. *J. Chem. Phys.* **1998**, *109*, 8161–8167.
- (82) Cruz, F. G.; Lam, K.-C.; Burke, K. Exchange-Correlation Energy Density from Virial Theorem. *J. Phys. Chem. A* **1998**, *102*, 4911–4917.
- (83) Maier, T. M.; Haasler, M.; Arbuznikov, A. V.; Kaupp, M. New approaches for the calibration of exchange-energy densities in local hybrid functionals. *Phys. Chem. Chem. Phys.* **2016**, *18*, 21133–21144.
- (84) Tao, J.; Staroverov, V. N.; Scuse-ria, G. E.; Perdew, J. P. Exact-exchange energy density in the gauge of a semilocal density-functional approximation. *Phys. Rev. A* **2008**, *77*, 012509.
- (85) Haasler, M.; Maier, T. M.; Grot-jahn, R.; Gückel, S.; Arbuznikov, A. V.; Kaupp, M. A Local Hybrid Functional with Wide Applicability and Good Balance between (De)Localization and Left-Right Correlation. *J. Chem. Theory Comput.* **2020**, *16*, 5645–5657.
- (86) Wodyński, A.; Arbuznikov, A. V.; Kaupp, M. Local hybrid functionals augmented by a strong-correlation model. *J. Chem. Phys.* **2021**, *155*, 144101.
- (87) Kong, J.; Proynov, E. Density Functional Model for Nondynamic and Strong Correlation. *J. Chem. Theory Comput.* **2016**, *12*, 133–143.

- (88) Becke, A. D. Density functionals for static, dynamical, and strong correlation. *J. Chem. Phys.* **2013**, *138*, 074109.
- (89) Lehtola, S.; Steigemann, C.; Oliveira, M. J. T.; Marques, M. A. L. Recent developments in LIBXC—a comprehensive library of functionals for density functional theory. *SoftwareX* **2018**, *7*, 1–5.
- (90) Dunning, T. H. Gaussian basis sets for use in correlated molecular calculations. I. The atoms boron through neon and hydrogen. *J. Chem. Phys.* **1989**, *90*, 1007.
- (91) Kendall, R. A.; Dunning, T. H.; Harrison, R. J. Electron affinities of the first-row atoms revisited. Systematic basis sets and wave functions. *J. Chem. Phys.* **1992**, *96*, 6796.
- (92) Woon, D. E.; Dunning, T. H. Gaussian basis sets for use in correlated molecular calculations. III. The atoms aluminum through argon. *J. Chem. Phys.* **1993**, *98*, 1358.
- (93) Woon, D. E.; Dunning, T. H. Gaussian basis sets for use in correlated molecular calculations. V. Core-valence basis sets for boron through neon. *J. Chem. Phys.* **1995**, *103*, 4572.
- (94) Peterson, K. A.; Dunning, T. H. Accurate correlation consistent basis sets for molecular core–valence correlation effects: The second row atoms Al–Ar, and the first row atoms B–Ne revisited. *J. Chem. Phys.* **2002**, *117*, 10548.
- (95) Prascher, B. P.; Woon, D. E.; Peterson, K. A.; Dunning, T. H.; Wilson, A. K. Gaussian basis sets for use in correlated molecular calculations. VII. Valence, core-valence, and scalar relativistic basis sets for Li, Be, Na, and Mg. *Theor. Chem. Acc.* **2011**, *128*, 69–82.
- (96) Ditchfield, R. Molecular Orbital Theory of Magnetic Shielding and Magnetic Susceptibility. *J. Chem. Phys.* **1972**, *56*, 5688.
- (97) Becke, A. D. A multicenter numerical integration scheme for polyatomic molecules. *J. Chem. Phys.* **1988**, *88*, 2547–2553.
- (98) Treutler, O.; Ahlrichs, R. Efficient molecular numerical integration schemes. *J. Chem. Phys.* **1995**, *102*, 346.
- (99) TURBOMOLE User’s Manual, https://www.turbomole.org/downloads/doc/Turbomole_Manual_76.pdf, accessed 27 October 2023.
- (100) Bahmann, H.; Kaupp, M. Efficient Self-Consistent Implementation of Local Hybrid Functionals. *J. Chem. Theory Comput.* **2015**, *11*, 1540–1548.
- (101) Liu, F.; Kong, J. Efficient Computation of Exchange Energy Density with Gaussian Basis Functions. *J. Chem. Theory Comput.* **2017**, *13*, 2571–2580.
- (102) Laqua, H.; Kussmann, J.; Ochsenfeld, C. Efficient and Linear-Scaling Seminumerical Method for Local Hybrid Density Functionals. *J. Chem. Theory Comput.* **2018**, *14*, 3451–3458.
- (103) Holzer, C. An improved seminumerical Coulomb and exchange algorithm for properties and excited states in modern density functional theory. *J. Chem. Phys.* **2020**, *153*, 184115.
- (104) Weigend, F. Accurate Coulomb-fitting basis sets for H to Rn. *Phys. Chem. Chem. Phys.* **2006**, *8*, 1057–1065.
- (105) Stoychev, G. L.; Auer, A. A.; Izsák, R.; Neese, F. Self-Consistent Field Calculation of Nuclear Magnetic Resonance Chemical Shielding Constants Using Gauge-Including Atomic Orbitals and Approximate Two-Electron Integrals. *J. Chem. Theory Comput.* **2018**, *14*, 619–637.
- (106) Reiter, K.; Mack, F.; Weigend, F. Calculation of magnetic shielding constants with meta-GGA functionals employing

- the multipole-accelerated resolution of the identity: implementation and assessment of accuracy and efficiency. *J. Chem. Theory Comput.* **2018**, *14*, 191–197.
- (107) Lehtola, S. Straightforward and Accurate Automatic Auxiliary Basis Set Generation for Molecular Calculations with Atomic Orbital Basis Sets. *J. Chem. Theory Comput.* **2021**, *17*, 6886–6900.
- (108) Lehtola, S. Automatic Generation of Accurate and Cost-Efficient Auxiliary Basis Sets. *J. Chem. Theory Comput.* **2023**, *19*, 6242–6254.
- (109) Pedersen, T. B.; Lehtola, S.; Galván, I. F.; Lindh, R. The versatility of the Cholesky decomposition in electronic structure theory. *Wiley Interdiscip. Rev. Comput. Mol. Sci.* **2023**, e1692.
- (110) Bast, R. Numgrid: Numerical integration grid for molecules. April 2020; <https://doi.org/10.5281/zenodo.1470276>.
- (111) Lindh, R.; Malmqvist, P.-Å.; Gagliardi, L. Molecular integrals by numerical quadrature. I. Radial integration. *Theor. Chem. Acc.* **2001**, *106*, 178–187.
- (112) Lebedev, V. I. A quadrature formula for the sphere of 59th algebraic order of accuracy. *Russ. Acad. Sci. Dokl. Math.* **1995**, *50*, 283–286.
- (113) GIMIC, version 2.0, a current density program. Can be freely downloaded from <https://github.com/qmcurrents/gimic> and <https://zenodo.org/record/8180435>.
- (114) The Numgrid program. It can be freely downloaded from <https://github.com/dftlibs/numgrid> and <https://zenodo.org/record/4815722>.
- (115) Arbuznikov, A. V.; Kaupp, M. Towards improved local hybrid functionals by calibration of exchange-energy densities. *J. Chem. Phys.* **2014**, *141*, 204101.
- (116) Arbuznikov, A. V.; Kaupp, M. Importance of the correlation contribution for local hybrid functionals: Range separation and self-interaction corrections. *J. Chem. Phys.* **2012**, *136*, 014111.
- (117) Bahmann, H.; Rodenberg, A.; Arbuznikov, A. V.; Kaupp, M. A thermochemically competitive local hybrid functional without gradient corrections. *J. Chem. Phys.* **2007**, *126*, 011103.
- (118) Kaupp, M.; Bahmann, H.; Arbuznikov, A. V. Local hybrid functionals: An assessment for thermochemical kinetics. *J. Chem. Phys.* **2007**, *127*, 194102.
- (119) Arbuznikov, A. V.; Kaupp, M. Local hybrid exchange-correlation functionals based on the dimensionless density gradient. *Chem. Phys. Lett.* **2007**, *440*, 160–168.
- (120) Perdew, J. P.; Staroverov, V. N.; Tao, J.; Scuseria, G. E. Density functional with full exact exchange, balanced nonlocality of correlation, and constraint satisfaction. *Phys. Rev. A* **2008**, *78*, 052513.
- (121) Johnson, E. R. Local-hybrid functional based on the correlation length. *J. Chem. Phys.* **2014**, *141*, 124120.
- (122) Mardirossian, N.; Head-Gordon, M. Mapping the genome of meta-generalized gradient approximation density functionals: The search for B97M-V. *J. Chem. Phys.* **2015**, *142*, 074111.
- (123) Van Voorhis, T.; Scuseria, G. E. A novel form for the exchange-correlation energy functional. *J. Chem. Phys.* **1998**, *109*, 400.
- (124) Yu, H. S.; He, X.; Truhlar, D. G. MN15-L: A New Local Exchange-Correlation Functional for Kohn–Sham Density Functional Theory with Broad Accuracy for Atoms, Molecules, and Solids. *J. Chem. Theory Comput.* **2016**, *12*, 1280–1293.

- (125) Tao, J.; Perdew, J. P.; Staroverov, V. N.; Scuseria, G. E. Climbing the Density Functional Ladder: Nonempirical Meta-Generalized Gradient Approximation Designed for Molecules and Solids. *Phys. Rev. Lett.* **2003**, *91*, 146401.
- (126) Perdew, J. P.; Tao, J.; Staroverov, V. N.; Scuseria, G. E. Meta-generalized gradient approximation: Explanation of a realistic nonempirical density functional. *J. Chem. Phys.* **2004**, *120*, 6898.
- (127) Zhao, Y.; Truhlar, D. G. A new local density functional for main-group thermochemistry, transition metal bonding, thermochemical kinetics, and noncovalent interactions. *J. Chem. Phys.* **2006**, *125*, 194101.
- (128) Boese, A. D.; Handy, N. C. New exchange-correlation density functionals: The role of the kinetic-energy density. *J. Chem. Phys.* **2002**, *116*, 9559–9569.
- (129) Zhao, Y.; Truhlar, D. G. Design of Density Functionals That Are Broadly Accurate for Thermochemistry, Thermochemical Kinetics, and Nonbonded Interactions. *J. Phys. Chem. A* **2005**, *109*, 5656.
- (130) Zhao, Y.; Truhlar, D. G. The M06 suite of density functionals for main group thermochemistry, thermochemical kinetics, noncovalent interactions, excited states, and transition elements: two new functionals and systematic testing of four M06-class functionals and 12 other functionals. *Theor. Chem. Acc.* **2008**, *120*, 215.
- (131) Yu, H. S.; He, X.; Li, S. L.; Truhlar, D. G. MN15: A Kohn–Sham global-hybrid exchange-correlation density functional with broad accuracy for multi-reference and single-reference systems and noncovalent interactions. *Chem. Sci.* **2016**, *7*, 5032–5051.
- (132) Stephens, P. J.; Devlin, F. J.; Chabalowski, C. F.; Frisch, M. J. Ab Initio Calculation of Vibrational Absorption and Circular Dichroism Spectra Using Density Functional Force Fields. *J. Phys. Chem.* **1994**, *98*, 11623.
- (133) Hertwig, R. H.; Koch, W. On the parameterization of the local correlation functional. What is Becke-3-LYP? *Chem. Phys. Lett.* **1997**, *268*, 345–351.
- (134) Becke, A. D. A new mixing of Hartree–Fock and local density-functional theories. *J. Chem. Phys.* **1993**, *98*, 1372.
- (135) Mardirossian, N.; Head-Gordon, M. ω B97M-V: A combinatorially optimized, range-separated hybrid, meta-GGA density functional with VV10 nonlocal correlation. *J. Chem. Phys.* **2016**, *144*, 214110.
- (136) Mardirossian, N.; Head-Gordon, M. ω B97X-V: A 10-parameter, range-separated hybrid, generalized gradient approximation density functional with nonlocal correlation, designed by a survival-of-the-fittest strategy. *Phys. Chem. Chem. Phys.* **2014**, *16*, 9904–9924.
- (137) Lehtola, S. Meta-GGA Density Functional Calculations on Atoms with Spherically Symmetric Densities in the Finite Element Formalism. *J. Chem. Theory Comput.* **2023**, *19*, 2502–2517.
- (138) Lehtola, S. Atomic Electronic Structure Calculations with Hermite Interpolating Polynomials. *J. Phys. Chem. A* **2023**, *127*, 4180–4193.
- (139) Ruud, K.; Helgaker, T.; Jørgensen, P. The effect of correlation on molecular magnetizabilities and rotational g tensors. *J. Chem. Phys.* **1997**, *107*, 10599.
- (140) van Wüllen, C. Die Berechnung magnetischer Eigenschaften unter Berücksichtigung der Elektronenkorrelation: Die Multikonfigurations-Verallgemeinerung der IGLO Methode.

Dissertation, Ruhr-Universität Bochum,
1992.

- (141) Janesko, B. G.; Proynov, E.; Kong, J.; Scalmani, G.; Frisch, M. J. Practical Density Functionals beyond the Overdelocalization–Underbinding Zero-Sum Game. *J. Phys. Chem. Lett.* **2017**, *8*, 4314–4318.

TOC Graphic

